sustainability

MDPI

Article

Smart Charging for Electric Car-Sharing Fleets Based on Charging Duration Forecasting and Planning

Francesco Lo Franco [1,*], Vincenzo Cirimele [1], Mattia Ricco [1], Vitor Monteiro [2], Joao L. Afonso [2] and Gabriele Grandi [1]

[1] Department of Electrical, Electronic and Information Engineering, University of Bologna, 40136 Bologna, Italy
[2] Department of Industrial Electronics, University of Minho, Azurem, 4800-058 Guimarães, Portugal
* Correspondence: francesco.lofranco2@unibo.it

Abstract: Electric car-sharing (ECS) is an increasingly popular service in many European cities. The management of an ECS fleet is more complex than its thermal engine counterpart due to the longer "refueling" time and the limited autonomy of the vehicles. To ensure adequate autonomy, the ECS provider needs high-capacity charging hubs located in urban areas where available peak power is often limited by the system power rating. Lastly, electric vehicle (EV) charging is typically entrusted to operators who retrieve discharged EVs in the city and connect them to the charging hub. The timing of the whole charging process may strongly differ among the vehicles due to their different states of charge on arrival at the hub. This makes it difficult to plan the charging events and leads to non-optimal exploitation of charging points. This paper provides a smart charging (SC) method that aims to support the ECS operators' activity by optimizing the charging points' utilization. The proposed SC promotes charging duration management by differently allocating powers among vehicles as a function of their state of charge and the desired end-of-charge time. The proposed method has been evaluated by considering a real case study. The results showed the ability to decrease charging points downtime by 71.5% on average with better exploitation of the available contracted power and an increase of 18.8% in the average number of EVs processed per day.

Keywords: electric vehicles; sustainable mobility; smart charging; electric car-sharing; charging management system; battery model; power flows forecasting; operation modes

Citation: Lo Franco, F.; Cirimele, V.; Ricco, M; Monteiro, V.; Afonso, J.L.; Grandi, G. Smart Charging for Electric Car-Sharing Fleets Based on Charging Duration Forecasting and Planning. *Sustainability* **2022**, *14*, 12077. https://doi.org/10.3390/su141912077

Academic Editors: Marc A. Rosen and Mouloud Denai

Received: 4 August 2022
Accepted: 16 September 2022
Published: 24 September 2022

1. Introduction

As stated in the European Green Deal, the European Union aims to be climate-neutral by 2050. This means achieving an economy with net-zero greenhouse gas emissions [1]. The massive adoption of renewable energy sources (RESs) and the passage to electric mobility are seen as fundamental actions in this process. However, many researchers are pointing out that an excessive penetration of RESs can lead to an intolerable decrease in the flexibility and reliability of the electrical grid. This is mainly due to the non-schedulability of RESs' energy production [2,3]. Along with this, the charge of electric vehicles (EVs) requires an increase in energy demand as well as the management of intermittent loads characterized by high power peaks. Furthermore, this kind of load is often unlikely to match the generation profile of RES.

Smart charging (SC) techniques are seen as a possible solution to address these issues. The term smart charging identifies all those strategies that act on the regulation of power flows required for EV charging to improve matching between the efficient electric grid usage and the charging needs. Often, SC techniques deal also with the effective integration of RESs. Several works on SC are available in the literature. In [4], the authors provide an SC method capable of modulating the power consumption of each charging point (CP) of a charging hub (CH) to optimize the integration with local photovoltaic production. This SC aimed to maximize self-consumption by minimizing the power exchanges with the

electrical grid. Similar purposes characterize the SC methods developed in [5,6]. These works describe an SC management system capable of allocating power among the EVs connected to the CPs of a CH. In addition to the self-consumption maximization, this SC method aimed to ensure an overall good state of charge (SOC) at departure time for all the vehicles in the CH. In [7], the developed SC method aimed at controlling EV consumption in relation to the variations in electricity price. The target was the reduction of the impact of EV charging on the electrical distribution network along with the minimization of charging costs. More recent works, such as [8,9], investigate the use of SC methods in the presence of bi-directional power flow exchange between the electrical grid and the vehicle batteries. In this case, the energy stored in the vehicle battery is used to provide ancillary services such as frequency regulation or can supply external load [10,11].

The use of smart charging is becoming more and more important in urban settings. In such a context, the development of electric mobility makes it possible to drastically reduce pollutant emissions with a significant positive social impact [12]. In large cities, where private mobility is a major source of pollutants [13,14] and greenhouse gases emissions [15], the introduction of alternative mobility solutions is becoming more common [16–18]. Among these, electric car-sharing (ECS) services are becoming increasingly popular. In particular, ECS adoption is growing in major European cities, where enforced regulations such as low emission zones are becoming increasingly popular [19–21].

However, the management of an electric car fleet is much more complex than its counterpart based on internal combustion engines. As is well known, this is due to the long time required for recharging and the limited range currently offered by traction batteries. To ensure adequate range for the whole fleet, the ECS provider needs large charging hubs equipped with a high number of charging points. These CHs have to be located inside the urban area, where the available peak power is often limited by the actual capabilities of the distribution network. EV charging is typically entrusted to human operators who retrieve the EVs within the city, transport them to charging hubs, and connect them to the CPs. Hence, the timing of the charging process may strongly differ among the vehicles due to their different state of charge (SOC) on arrival at the CH. This leads to non-optimal exploitation of the charging points, as many EVs remain connected even after being fully charged. This means that several CPs remain inactive for a long time.

The aforementioned issues have been addressed in some previous works. In [22], the authors developed a method to model the operator-controlled charging operations and customers' EV picking behavior. This model was used to understand how to manage the charge of the fleet to make electric car-sharing viable and profitable. Similar considerations were made in [23,24] that focused on the optimization of the CHs layout and location. However, none of these works address the adoption of SC methods. SCs for EV-shared fleets are instead discussed in [25,26]. In [25], the SC works by shifting the electricity demand for the recharge away from high-priced peak hours, attempting to match the profile of RESs production. In [26], the SC operates by shifting the usage of shared EVs through a designed dynamic pricing scheme, with the objective of maximizing the ECS provider's profit.

Although these works demonstrate how the adoption of SC techniques can reduce the overall cost of charging operations, they do not address the issue of fleet management and charging in relation to operators' time schedules. In particular, no strategy is employed to synchronize operators' handover cycles to and from the CHs with the EVs' charging time. Indeed, this missing synchronization may introduce a slowdown in operator activities, non-optimal exploitation of the available power, and a reduction in the number of EVs charged per day.

This paper presents an SC method, specifically devoted to electric car-sharing charging hubs, which aims to overcome the aforementioned limits. The developed method allows for minimizing the uncertainty as to the duration of charging and synchronizing it with the typical time schedule of ECS operators. This SC would lead to a contemporary increase in the number of vehicles processed per day and improve the exploitation of the available CPs.

Differently from the other charging management systems, where all connected EVs receive the same amount of power, the proposed SC method acts on the management of charging duration by controlling the power required by each single charging point according to the state of charge of the vehicle and the desired end-of-charge time. At the same time, the proposed SC controls the total power consumption of the CH by preventing the power demand from exceeding the power available at the grid connection point and maximizing the exploitation of the available contracted power.

These goals are achieved by dynamically regulating the power consumption of each connected EV by means of the power set-point modulation of each CP. The power set-point results from a battery charging behavioral model (BCBM) that forecasts the value of power that the CP has to deliver to the EV to complete the charging within a time interval chosen by the ECS operator. The BCBM dynamically updates the forecast of the charging power on the base of the evolution of the SOC and the charging rate (C-rate) during the charging process.

The proposed SC stems from a real case study scenario and collaboration with the ECS provider of the city of Bologna, Italy, named "Corrente" [27]. The effectiveness of the developed SC is assessed by comparing it with the standard charging procedure currently adopted for the management of the Corrente CHs. Results show performance improvements in terms of the number of EVs reaching the full charge in the scheduled time, more effective exploitation of the available contracted power level, reduction of the overall fleet charging times, and increased number of EVs that operators can process during an entire work cycle.

The paper is structured as follows: Section 2 analyzes the case study and the possible issues arising from managing a large ECS fleet. Section 3 describes the EV battery charging behavioral model and the algorithm used to simulate the power demand profiles of the CH. Section 4 provides the SC method. The results and the comparison between the proposed SC and the standard method are discussed in Section 5. Finally, conclusions are reported in Section 6.

2. Description of the Reference Case Study

The car-sharing fleet of the cities of Bologna and Ferrara consists of 335 EVs displaced over the whole metropolitan area. Users can book the vehicle through a dedicated mobile app, drive, and park the vehicle within a specific perimeter. The covered area in the municipality of Bologna is shown in Figure 1. The car-sharing fleet is entirely composed of battery EVs. About 70% of the fleet is made by ZOE ZE50 R135 (2020) equipped with a battery pack having a capacity of 52 kWh. The remaining vehicles are ZOE ZE40 R110 (2018) equipped with a 41 kWh battery pack.

The ECS provider remotely monitors the SOC and the location of each vehicle. When the SOC of a vehicle drops below a certain level, an ECS operator drives it toward a charging hub to recharge the EV's battery. When the vehicle is fully charged, the operator disconnects it from the charging station and returns it to one of the dedicated parking spots, making it available for new users. It is essential to point out that this operation is not based on rigid procedures. Indeed, an operator is left free to bring a vehicle to the charging hub even if the vehicle's battery does not strictly need to be recharged. This approach aims to have the user find a vehicle as charged as possible so as to ensure the maximum possible range and limit the so-called user range anxiety [12,25]. For each EV, the different phases of the charging procedure can be summarized as follows: (a) the operator locates the vehicle to be recharged and drives it toward the CH; (b) the operator connects the EV to a charging station of the hub, starting the battery charging; (c) the SOC of the EV battery reaches a satisfactory level (qualitatively around 100%), hence, the operator disconnects the vehicle and brings it back to the closest free parking lot.

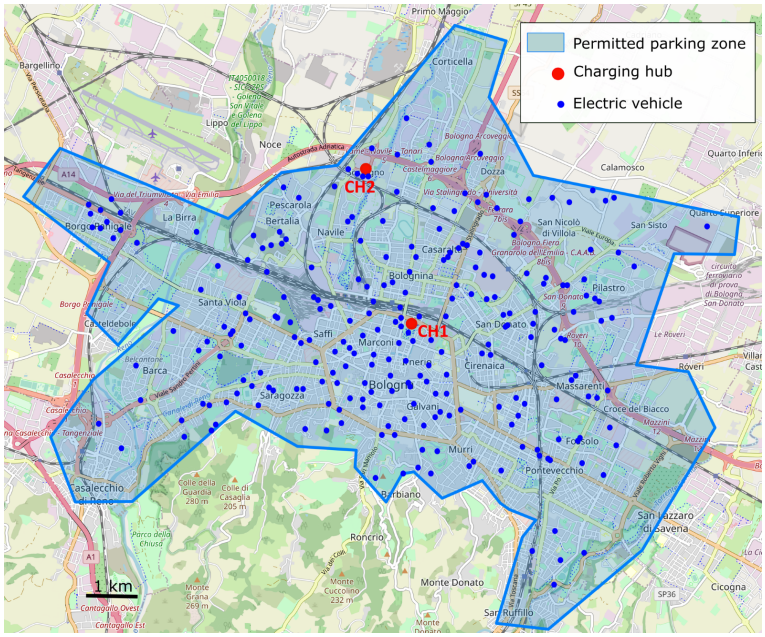

Figure 1. Map of electric car-sharing fleet operation area within the municipality of Bologna. The blue area represents the area allowed for vehicle use and parking. The red points indicate the location of the charging hubs. The blue points represent real-time locations of the car-sharing EVs. Map adapted from [28].

In the city of Bologna, there are two charging hubs, represented by the red markers in Figure 1. A CH consists of a parking area equipped with AC charging stations. The CH located in the city center, labeled as CH1, contains four charging stations, each with two 22 kW Type 2 connectors (i.e., a total of eight charging points of 22 kW each). The CH, located in a more peripheral area of the city—namely, CH2—has six charging stations for a total of twelve 22 kW charging points. In the continuation of the work, reference will be made only to CH1 for the sake of simplicity and synthesis.

The blue points in the map depict the possible location of the EVs around the city. As visible from Figure 1, the distance between a parked EV and the CH is practically random and strongly differs among the vehicles. Consequently, the time corresponding to completing the whole charging procedure, which includes phase (a), phase (b), and phase (c), can be different from vehicle to vehicle. Equation (1) defines the duration of the entire charging procedure, indicated as T_{CP}, by discerning the contribution of the three phases:

$$T_{CP} = T_a + T_b + T_c \quad (1)$$

The average value of $T_a + T_c$ is 40 min; however, there is large variation around the average as the duration of phase (a) (T_a) and the duration of phase (c) (T_c) for each vehicle depend on the distance from the charging hub and the traffic conditions. T_b represents the time interval during which the vehicle remains plugged to the charging point. It depends on the EV battery capacity, the charging power, and the state of charge at the beginning of the charging process SOC_0. Since the vehicle model population is fairly homogeneous (it includes only 41 kWh or 52 kWh batteries), and all charging points have a rated power of 22 kW, the variation of T_b among the different vehicles of the fleet mainly depends on the values of SOC_0 upon their arrival at the CH.

Clearly, SOC_0 is generally different from vehicle to vehicle. This appears evident by analyzing the data reported in Figure 2, which show the SOC_0 distribution of the vehicles arriving at CH1 over three months (i.e., about 1650 charging events). These data are monitored and collected by the ECS provider for each charging event and made available on a dedicated online platform. The scatter plot in Figure 2a reports the SOC_0 value for each charging event in relation to the vehicle model. The dark blue markers refer to the

ZOE ZE40, and the light blue markers to the ZOE ZE50. The black curve in the figure shows the probability density function (pdf) obtained from Gaussian kernel density estimation that is associated with the SOC_0, whose value is readable on the right y-axis.

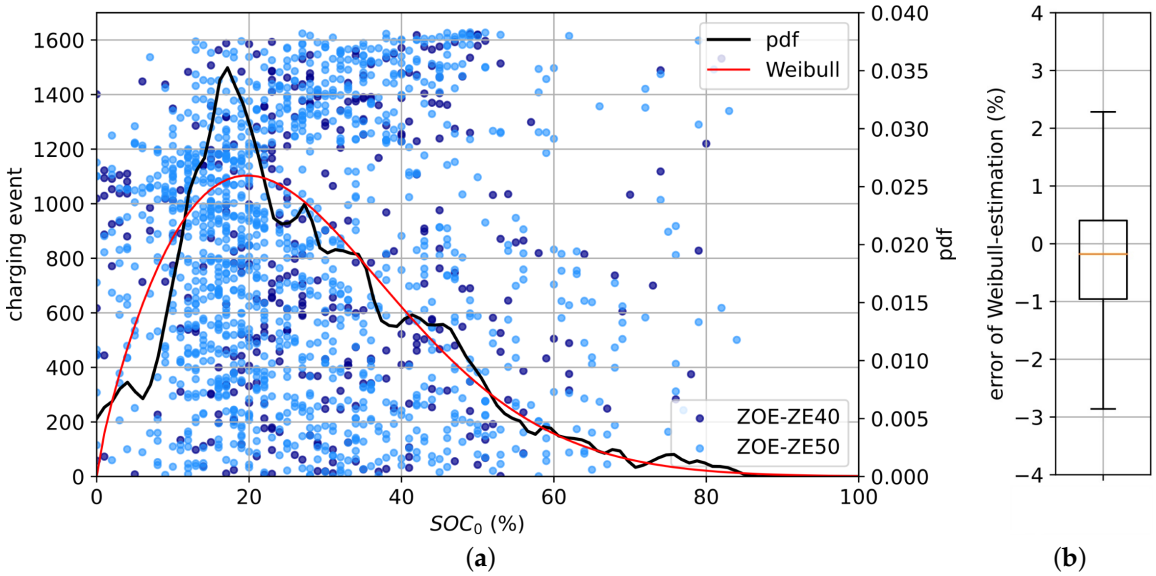

Figure 2. State of charge data of the CH1 collected over a period of 3 months. (**a**) SOC_0 values in relation to the vehicle model: the dark blue markers refer to the ZOE ZE40, the light blue markers refer to the ZOE ZE50. The black line shows the related pdf, and the red line represents the pdf estimation based on a Weibull function. (**b**) Boxplot of the error introduced by the Weibull function approximation.

The average value of the registered initial SOC of the examined population is $SOC_{0m} = 27\%$ with standard deviation $SOC_{0std} = 16\%$. This distribution can be conveniently associated to a Weibull distribution (red curve in Figure 2a having $k = 1.8\%$ and $\lambda = 31\%$). The boxplot of Figure 2b shows the error introduced by the Weibull function estimation via a root-mean-square error (RMSE) that is equal to about 1.25%.

For each charging, the dataset made available to the ECS provider gives the following information:

- The ID number of the EV;
- The EV model;
- The ID number of the charging point (CP) belonging to the CH;
- The state of charge SOC_0 (pre-charging SOC);
- The state of charge at the end of the charging process, SOC_{end} (post-charging SOC);
- The start timestamp of the charging process, t_{start} (when the vehicle is connected to the charging point);
- The timestamp of the end-of-connection. t_{end} (when the vehicle is disconnected from the charging point).

Note that t_{end} may not coincide with the end-of-charge time t_{ech}. In fact, the vehicle may be disconnected even a long time after reaching the maximum SOC on the basis of operator availability. An example of the provided data frame format is reported in Table 1. By analyzing the main data frame, it is possible to extrapolate some noteworthy characteristics related to the charging processes of the charging hubs. Figure 3a reports the frequency distribution of the levels of SOC_0 and SOC_{end}. Differently from SOC_0, the SOC_{end} values are more concentrated on their average value (i.e., 98%). The orange plot in Figure 3a shows that almost all vehicles are disconnected when the SOC is higher than 90%. The violin plots of Figure 3b show the distribution of t_{start}, t_{end}, and the connection period T_b. The start-charging events occur in the 7:00–20:00 time range, which corresponds to the working time of the ECS operators. On the other hand, the t_{end} occurrences present

two main clusters. The first cluster is related to vehicles that are disconnected on the same day of t_{start}. The second cluster is related to vehicles disconnected the day after the t_{start} (that is, vehicles charged overnight). These distributions reflect on the connection time, which is calculated as the difference between t_{end} and t_{start}. The average connection time of the over-day (OD) charges is 3.2 h while the vehicles subjected to overnight (ON) charging remain connected for 15 h on average.

Table 1. Example of the first three rows of the data frame provided by the ECS company.

EV ID	EV Model	CH ID	CP ID	SOC_0	SOC_{end}	t_{start}	t_{end}
34	ZE40	CH1	3	13%	98%	13 December 2021 08:49:45	13 December 2021 10:06:51
107	ZE50	CH1	2	25%	100%	13 December 2021 09:12:45	13 December 2021 11:02:11
12	ZE50	CH1	1	8%	97%	13 December 2021 08:00:05	13 December 2021 09:01:22

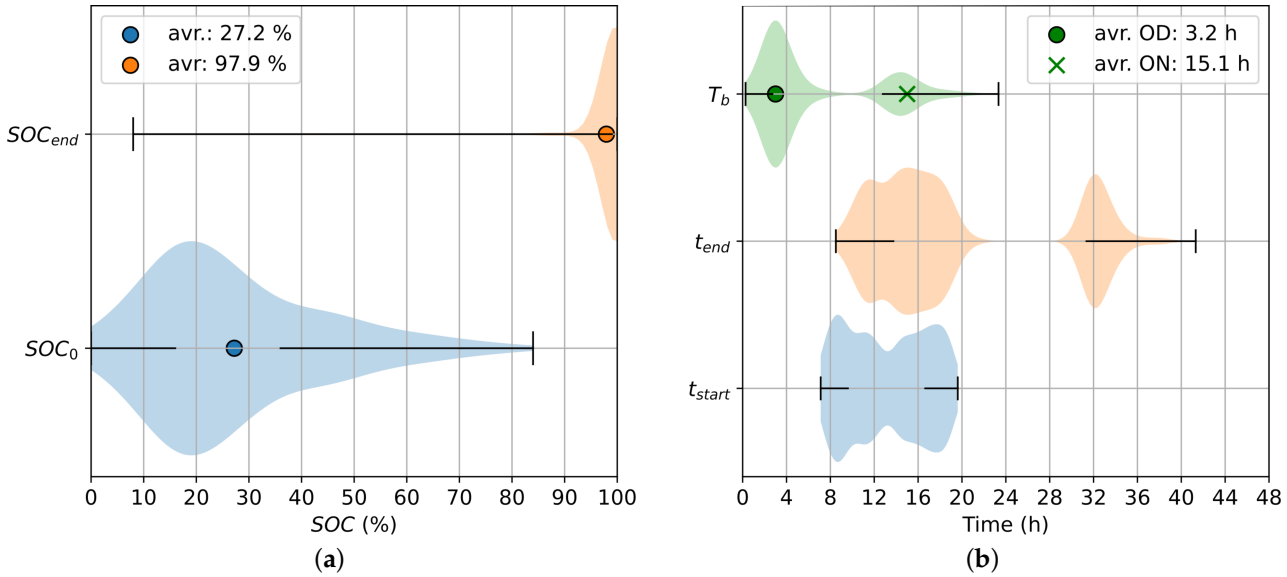

Figure 3. Statistical processing of the ECS data frame represented via violin plots. (**a**) Distribution of SOC_0 and SOC_{end}; (**b**) t_{start}, t_{end}, and T_b distribution. Markers in the figures represent the mean value of quantities.

As shown in Table 1, the available data do not give a direct indication of charging time and instantaneous power, while it is possible to extrapolate the energy supplied during charging from the knowledge of the initial and final SOC.

3. EV Charging Power Modeling and Management System

This section analyzes the characteristics of the current charging hub power flow and presents the models adopted to perform the comparative analysis against the charging method proposed in this paper.

3.1. Current EV Charging Management System

The total power required by the charging hub (P_{CH}) is

$$P_{CH}(t) = \sum_{i}^{N_{ch}} P_{EVi}(t) \quad (2)$$

where P_{EVi} is the charging power provided to the $i-th$ EV and N_{ch} is the number of vehicles connected to the charging stations at time t. According to the characteristics of the electric distribution network supplying the CH, the available maximum power $P_{\text{CHmax}} = 100$ kW (i.e., the contracted power) is lower than the sum of the rated powers of the charging stations P_{CPi} installed in the hub. Hence,

$$\sum_i P_{CPi} > P_{\text{CHmax}} \tag{3}$$

The actual management system acts by reducing the power consumption of each CP in case the requested power of the whole CH exceeds P_{CHmax}. In the CH under analysis, the charging management system (CMS) operates according to the following equation set:

$$P_{CPi}(t) = \begin{cases} 22 \text{ kW} & \text{if } N_{ch} \leq 4 \\ \dfrac{P_{CHmax}}{N_{ch}} & \text{if } N_{ch} > 4 \end{cases} \tag{4}$$

In short, the management system simply lowers the power supplied uniformly for all charging vehicles when the required power exceeds the available power. Clearly, this operation leads to highly non-homogeneous charging profiles among the vehicles.

The charging profile is required to calculate the evolution of $P_{\text{CH}}(t)$ during the day. Unfortunately, the data about the charging profiles were not available to the ECS provider; hence, the power flow associated with each charge was reconstructed using the forecasting algorithm presented in [4] and discussed in this section.

3.2. Battery Charging Behavioral Model

In the case of AC charging stations, the power (referred to as P_{OBCh}) is controlled by the onboard power electronic converter [29], which influences the duration of the charge itself. The onboard chargers of the Renault ZOEs have a rating power of 22 kW equal to the maximum power provided by the CPs. Along with the modulation due to the management system, the charging profile of the vehicles is controlled to comply with the Constant Current–Constant Voltage (CC-CV) charging protocol for lithium batteries [30,31]. According to this protocol, the charge starts with the CC phase, where a constant current is provided to the battery. During this phase, the battery voltage increases, and the power profile follows that of the voltage. When the battery voltage reaches the upper cut-off value, the CV phase begins. During this phase, the onboard charger keeps the battery voltage constant while the charging current decreases. Therefore, the power profile follows the current drop. The CV phase continues until the end of the charge.

The CC-CV charging phases can be conveniently described through the power–SOC curves [32]. Let us consider a whole EV charging process, starting from SOC_{min} = 0% up to the full charge at SOC_{max} = 100%. In the beginning, the EV absorbs the power $P_{\text{EV}}(SOC_{\text{min}})$; then, the charging power increases as the SOC increases. This increase continues until a threshold value SOC_{CV} is reached. At this point, the power $P_{\text{EV}}(SOC_{\text{CV}})$ becomes equal to the peak value P_{EVmax} of the whole charging profile. The value of P_{EVmax} depends on both P_{CP} and the onboard charger power capability P_{OBCh} and corresponds to $P_{\text{EVmax}} = min[P_{\text{CP}}, P_{\text{OBCh}}]$. Once SOC_{CV} is reached, P_{EV} reduces until it goes to zero in correspondence of SOC_{max}.

Knowing the P_{EVmax} value, the charging power profile can be obtained as

$$P_{\text{EV}} = k\, P_{\text{EVmax}} \tag{5}$$

where $k \in [0, 1]$ is a normalization factor that varies during the charging process as a function of the SOC according to the following equation set:

$$k = \begin{cases} k_0 + \left(\dfrac{1-k_0}{SOC_{CV}}\right) SOC & \text{if } SOC \leq SOC_{CV} \quad (6a) \\ \left(\dfrac{SOC_{max} - SOC}{SOC_{max} - SOC_{CV}}\right)^{\alpha} & \text{if } SOC > SOC_{CV} \quad (6b) \end{cases}$$

A linear dependence between the SOC and the power is assumed in the CC phase (Equation (6a)) while a polynomial evolution, driven by the exponent α, is assumed for the CV phase (Equation (6b)). It can be seen that $k = k_0$ when $SOC = SOC_{min}$ (i.e., $P_{EV} = P_{EV}(SOC_{min})$), $k = 1$ when $SOC = SOC_{CV}$ (i.e., $P_{EV} = P_{EVmax}$), and $k = 0$ when $SOC = SOC_{max}$ (i.e., $P_{EV} = 0$).

Along with the SOC, the P_{EV} profile changes also as a function of the adopted charging rate (C-rate, C_R), i.e., the ratio between charging power and EV battery energy capacity C_B (expressed in kWh). In the referred charging process, the higher C_R is, the lower SOC_{CV} is. This happens because a higher charging current causes a higher voltage drop across the internal resistance of the battery. The cut-off voltage value is therefore reached faster and in correspondence with a lower SOC. This behavior is described by Equation (7), which provides the analytical expression of the SOC_{CV} as a function of C_R:

$$SOC_{CV}(C_R) = SOC_{CV}(C_{R0}) + \frac{dSOC_{CV}}{dC_R} C_R \quad (7)$$

where $SOC_{CV}(C_{R0})$ represents the value of SOC_{CV} of a charging process having a quasi-zero C-rate. In this condition, the battery voltage reaches the limit value at the end of the charging. In other terms, the charging process has only the CC phase; so, $SOC_{CV}(C_{R0}) = SOC_{max}$. The term $\frac{dSOC_{CV}}{dC_R} C_R$ introduces a deviation from $SOC_{CV}(C_{R0})$ for $C_R \neq C_{R0}$, where the derivative of SOC_{CV} with respect to C_R generally assumes negative values (i.e., SOC_{CV} decreases as C_R increases).

The internal battery voltage increase also affects the parameter k_0 in Equation (6a) as it expresses the ratio of $P_{EV}(SOC_{min})$ to P_{EVmax}. The dependency of k_0 on C_R is described by the following equation:

$$k_0(C_R) = k_0(C_{R0}) + \frac{dk_0}{dC_R} C_R, \quad (8)$$

where $k_0(C_{R0})$ is the value of k_0 for a quasi-zero C-rate charging process that implies an over-voltage on the battery's internal resistance close to zero. The limit value of $k_0(C_R)$ is the ratio between the battery open-circuit voltage and the CV cut-off voltage for C_R tending to C_{R0}.

As detailed in [33], different EV models may have different charging profiles. This is due to the differences in EV hardware (battery, onboard charger, etc.), and firmware (mainly, the battery management system) adopted by the different manufacturers. The charging profile models adopted in the present work, whose parameters refer to the Renault-ZOE EV, are retrieved from [34–37] for different C-rates. The different profiles are reported in Figure 4a and show the measured charging power P^*_{EV} as a function of the state of charge considering three different charging ratings P_{CP} of the CP: 7 kW, 22 kW, and 46 kW.

Starting from these real data, an optimal setting of the variables of Equations (6)–(9), i.e., the elements of the vector $\bar{a} = \left[\alpha, k_0(C_{R0}), \frac{dSOC}{dC_R}, \frac{dk_0}{dC_R}\right]$, are searched via an iterative deterministic process that considers all possible combinations of the elements of $\bar{a}$ within pre-determined ranges of variation. The search aims at identifying the set of parameters that minimize the RMS error between the reference P^*_{EV} and the output power obtained by the derived model. The obtained values of $\bar{a}$ are reported in Table 2 together with the value of the RMSE.

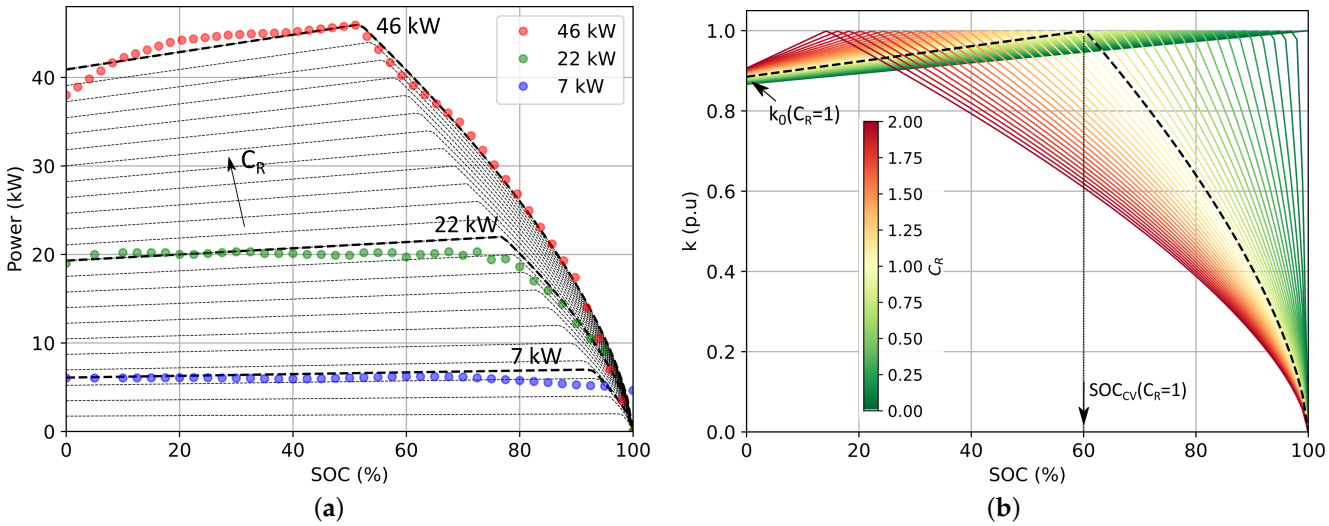

Figure 4. Sampled and predicted charging power profiles for the Renault-ZOE. (**a**) Comparison between the field-measured data (colored markers) and the predictions of the obtained model (black dashed lines). (**b**) Normalized charging power profile (k) as a function of the SOC and the C-rate. The dashed black line shows the value of SOC_{CV} and k_0 relating to $C_R = 1$.

Table 2. Obtained values of $\bar{a}$ parameters that minimize the RMSE with respect to the sampled Renault-ZOE charging profiles.

α	$k_0(C_{R0})$	$dSOC/dC_R$	dk_0/dC_R	RMSE
0.65	0.87	−42.85	0.02	0.88

The comparisons between the observed data and the model predictions are made visible in the same Figure 4a, where the power profile for different increasing C-rates is also depicted. Finally, Figure 4b shows the $k(\bar{a})$ profile as a function of SOC and C_R.

3.3. Charging Hub Power Flow Calculation

The model obtained as described in Section 3.2 is part of an algorithm that, starting from vehicle-specific data such as charging profile, state of charge, and starting and ending time of the charging process, is able to construct the aggregate load profile of the entire charging hub (Figure 5). The mentioned algorithm is based on the one presented in [4]. Its adapted version, which considers the battery charging behavioral model proposed in this paper, is here briefly summarized by the flow chart in Figure 5. In short, the algorithm calculates the charging power profile $P_{EV}(t)$ of each connected EV on the basis of the EV data (i.e., C_B and SOC_0) and the CH data (i.e., P_{CP} and N_{ch}), with a 1-min resolution. Having as input the time t_{start}, the algorithm is able to indicate if an EV is disconnected before having reached SOC_{max} (i.e., before full charge is reached) or if the vehicle remains connected for longer than necessary (i.e., t_{end} higher than end-of-charging time t_{ech}). The aggregate power of the whole CH is obtained as the sum of the power required by each charging point.

The algorithm has been applied to evaluate the total power demand of the reference scenario of the CH1 considering a typical day in December 2021. According to the results of the data analysis summarized in Figure 3b, the simulation time starts at 7:00 am. The obtained results are shown in Figure 6. Figure 6a shows the power provided by each charging point of CH1 to the EVs as a function of time. The connection instant t_{start} of each EV to the j-th CP and the disconnection instant t_{end} are indicated with the circular and triangular markers, respectively. The color of the markers indicate the EV's state of charge at t_{start} and t_{end}, respectively. The bar marker indicates the end-of-charging time t_{ech} forecasted by the developed model.

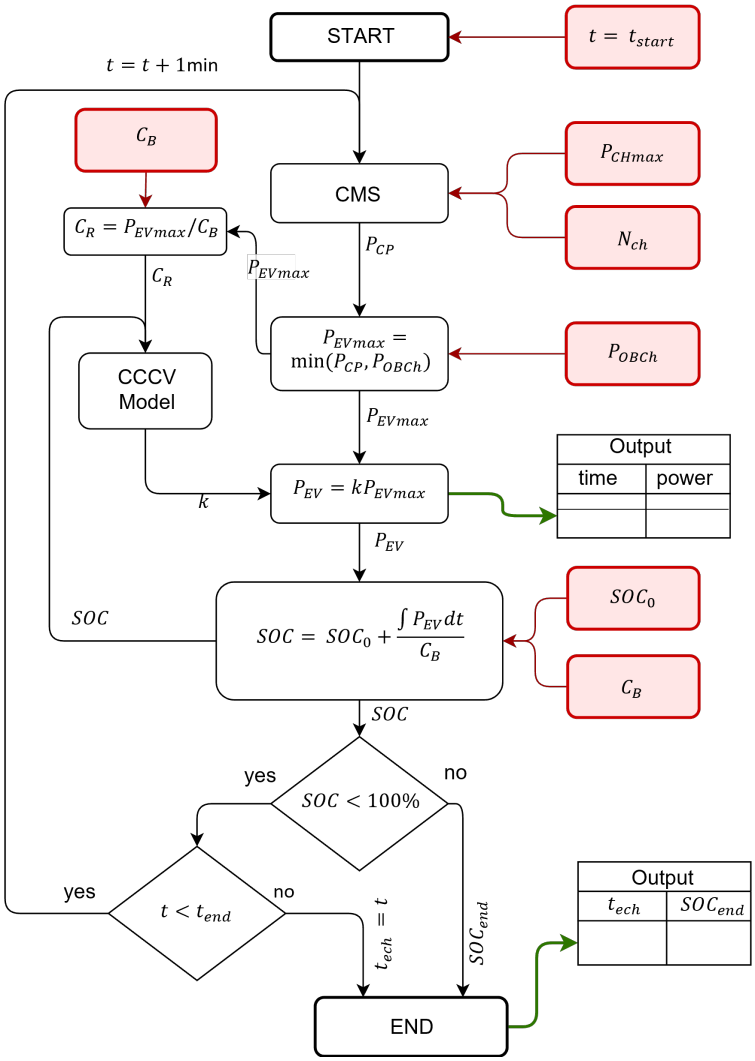

Figure 5. Flowchart of the EVs charging power flow calculation algorithm. The red boxes and related arrows represent the input data. The green arrows represent the collected output data.

It can be observed that, in addition to the overnight charges represented by the group of connected vehicles in the evening hours (after 18:00), the non-optimal condition ($t_{\text{end}} > t_{\text{ech}}$) can often occur in over-day charging as well (from 7:00 to 18:00). This working condition affects the performance of the whole charging hub. In fact, as can be seen in Figure 6b, the whole CH power rarely reaches its maximum value and the number of connected vehicles is always below its maximum capability. On the day considered, the CH provides 737 kWh to the EVs and the average CH power is 55 kW, which is well below its max availability.

The accuracy of the proposed model is assessed by comparing the information about the energy supplied to each vehicle that is available in the data frame of the ECS provider. By initializing the same SOC_{0i} for a certain charge event, the accuracy of the algorithm is evaluated by calculating the error between the $SOC(t_{\text{end}})$ obtained by the model and the one obtained by the measurements of the ECS provider. Simulations are carried out considering the whole data collection and using the SOC_0 values reported in Figure 2. The model results have reproduced the actual data with an RMSE = 2.64%.

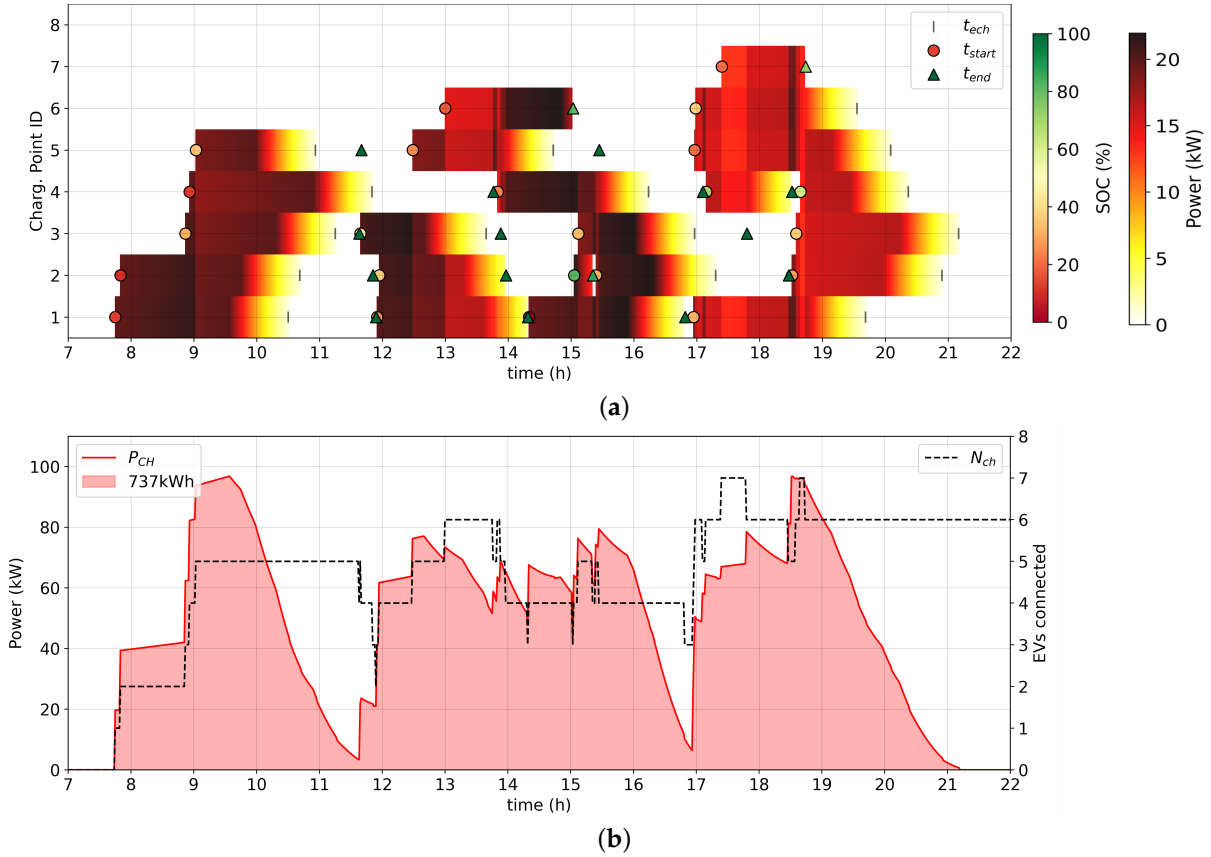

Figure 6. Representation of the actual power flows of the studied charging hub. (**a**) Power provided by each CP (indicated by the ID reported on y-axis) to the EVs. The round markers and triangular markers indicate the t_{start} and t_{end} instant of each connection, respectively. Their color represents the corresponding value of SOC. The bar-markers indicate the t_{ech} values. The evolution of the power flow during each charge is indicated through a colormap. (**b**) Power provided by the whole CH. The red area is the delivered energy. The dashed black line indicates the number of vehicles connected to the CPs of CH.

4. Smart Charging Method

The analysis carried out in Section 2 highlighted the high variability of the interval T_{b}, during which a vehicle remains plugged. This makes it difficult to plan a schedule in charging management, and often an EV remains connected for longer than necessary as the end of charging occurs in periods when the ECS operator is not present. This also leads to non-optimal exploitation of the charging hub as some charging points remain inactive even when a vehicle is connected. As a result, the average power used by the CH remains well below its maximum capability. Hence, the SC here proposed has been developed with the aim to improve the exploitation of the CH's available power and manage the charging processes in such a way to respond to precise time scheduling based on the ECS operator cycles of presence and absence in the CH. Differently from the starting scenario (i.e., the power management based on Equation (4)), where all connected EVs receive the same amount of power, the proposed SC promotes the management of charging duration by differently allocating powers among the EVs as a function of their state of charge and the desired end-of-charge time (t^*_{ech}). This means the SC substantially controls the duration of the time interval T_{b}, reducing the idle intervals of the CPs. As a side effect, this is also a means to increase the average power output of the CH and improve the exploitation of the available grid capabilities.

The proposed SC method modulates the power P_{EVi} delivered to the i-th EV by setting the j-th CP power to which the EV_i is connected. This modulation is based on the following equation set:

$$P_{CPj} = \begin{cases} 22 \text{ kW} & \text{if } N_{\text{ch}} \leq 4 \quad (9a) \\ \dfrac{\left(\dfrac{SOC_{\max} - SOC_{0i}}{100}\right) C_{Bi}}{\left(t^{*}_{ech,i} - t_{start,i}\right) \lambda_i} & \text{if } N_{ch} > 4 \quad (9b) \end{cases}$$

The numerator of Equation (9b) represents the energy that should be delivered to the EV_i to reach the full charge (i.e., $SOC_{\max}$) starting from its SOC_{0i}. The denominator represents the desired duration of the charge. The parameter λ is a corrective coefficient that considers the charging power variation due to the CC-CV protocol.

The role of λ can be conveniently described by referring to Figure 7a. This figure shows two charging events, both starting at $t_{start} = 0$ h and referring to the same EV model ZOE ZE50 and the same CP power rating $P_{\text{CP}} = 22$ kW. The first vehicle starts charging with an SOC of 60% and the second one with an SOC of 0%. Both EVs start the CV phase at $SOC = SOC_{\text{CV}} = 80\%$. The CV phase lasts about 1 h up to the full charging of the vehicles. According to the different starting SOCs, the CV phase for EV_1, over the entire charging duration, lasts longer than that for EV_2. As a result, the average power $\bar{P}_{\text{EV1}}$ of EV_1 is lower than $\bar{P}_{\text{EV2}}$. Furthermore, the average power $\bar{P}_{\text{EV}}$ provided to the vehicle depends on the CP output power. Finally, considering the same EV model, we can conclude that the higher P_{CP} is, the larger the share of the CV phase over the whole charging period, and the lower $\bar{P}_{\text{EV}}$ is compared to P_{CP}. All these correlations are summarized through the parameter λ, which can be defined as

$$\lambda(SOC_0, P_{\text{CP}}) = \frac{\bar{P}_{\text{EV}}(SOC_0, P_{\text{CP}})}{P_{\text{CP}}} \quad (10)$$

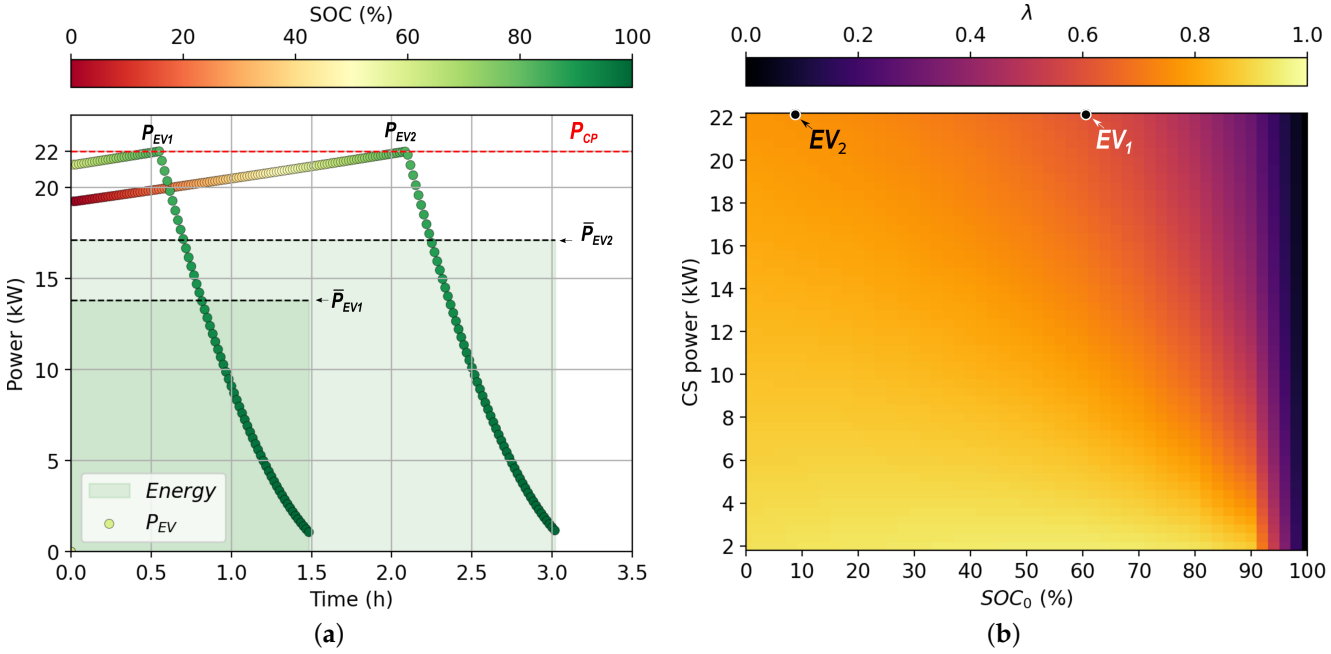

Figure 7. Graphical explanation of the λ coefficient: (**a**) Two charging events starting with different SOC_0 with the same P_{CP} (dashed red line). The colored dots show the EVs' power profiles and dashed black lines represent their respective average power. The green areas represent the energy supplied to the EVs. (**b**) λ values as a function of SOC_0 and P_{CP} for the ZOE ZE50. The markers show the λ value referring to the charging events of panel (**a**).

Figure 7b shows the values of λ as a function of SOC_0 and P_{CP} for the ZOE ZE50. In conclusion, Equation (9) sets the power that the CP has to provide to the EV to fully

charge it at the desired time (t^*_{ech}) and the λ coefficient allows to take into account the variation of P_{EV} due to the onboard charger modulation.

In order to comply with the maximum CP power limit and the maximum power available to the whole CH, the following constraints hold:

$$\begin{cases} P_{CPj} \leq 22 \text{ kW} \\ P_{\text{CH}} = \sum_{i=1}^{N_{\text{ch}}} P_{EVi} \leq P_{\text{CHmax}} \end{cases} \tag{11}$$

Attention has to be paid to the choice of $t^*_{ech,i}$: an under-setting of the desired charging period may lead to an overload of the charging hub, i.e., the violation of (11). To overcome this issue, the CMS constantly measures the CH consumption and increases $t^*_{ech,i}$ (i.e., decreases P_{CPj}), if constraints (11) are not met. Figure 8 shows the algorithm that calculates P_{CH} following the SC technique proposed in this section.

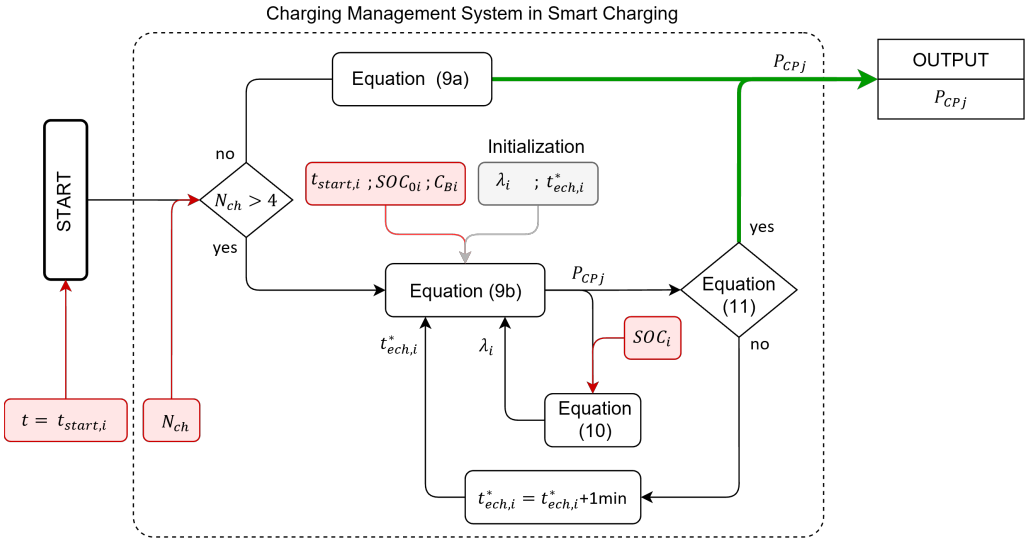

Figure 8. Flowchart of the proposed smart charging according to the equations described in this section. The red boxes are the data required as input to obtain the CP power set-point (green box). The gray box contains the initialization values of λ and t^*_{ech} required by Equation (9b).

From a technical point of view, the CMS needs to communicate with the charging stations of the CH, sending the value of P_{CP} for each CP. Then, the on-board charger receives the set-point of power from the CP connector and modulates the consumption accordingly. This procedure can be performed via the control pilot pin of the AC Type 2 connector (typical socket used in EU), which is responsible for the post-plug signaling. The control pilot communicates to the on-board charger the maximum power available to the CP via a PWM voltage signal, whose duty cycle is a function of the maximum current the CP can supply [38]. By dynamically modulating the control pilot duty cycle, it is possible to modulate the power of the on-board EV charger operating the SC.

5. Results

The comparison between the actual ECS provider charging management described by Equation (4) (hereafter referred to as St. C) and the proposed smart charging method based on Equation (9), has been performed by means of simulation starting from the same reference scenario described in Section 2.

5.1. Simulations Settings

The considered CH is equipped with eight CPs. The connection instant (t_{start}) of EVs to the CPs occurs only from 7:00 to 20:00, i.e., the working hours of the ECS operators.

Hence, no EVs are plugged in after 20:00, and the EVs that are not yet fully charged at that time are disconnected at 7:00 the following morning. The simulations considers two ECS operators working simultaneously during the day. Based on the average times given in Section 2, an operator is considered to arrive at the CH every 20 min. Hence, due to the availability of the operators to connect new EVs, the simulation setting considers that the time between two consecutive t_{start} cannot be less than 20 min. A two-minute interval is assumed as the time between the disconnection of a charged vehicle and the connection of a new vehicle to be recharged.

The activities of the two operators begin at 7:00, with all EVs left for overnight charging assumed as fully charged. From 7:00 onward, the connection time t_{start} to the CPs of subsequent EVs depends on the presence of the operators in the CH and the duration of the charging of the EVs previously connected. Once the eight CPs are occupied, the $t_{start,i}$ from the ninth vehicle onward will depend on the SOC reached by the vehicles already connected. Hence, starting from the ninth EV, the operator will directly connect it if at least one of the already connected vehicles is fully charged; otherwise, the operator has to wait until the full charge of one connected EV is reached. In summary, on the basis of Equation (9), the proposed SC method allocates the power to the CPs as a function of the connected EV SOC_0 to reach SOC_{max} within a specific reference time $t^*_{\text{ech}} = 20$ min that coincides with the average availability of the operators in the CH.

To perform the comparison between St. C. and the proposed SC, the simulations of both scenarios have the same initial conditions, i.e., the same EV models, the same t_{start} as the first set of EVs, and the same SOC_0. The SOC_0 of the vehicles at t_{start} is randomly selected among the samples of the data set shown in Figure 2.

5.2. Simulation Results

The results of the simulations comparing St. C and SC methods are summarized in Figure 9. In particular, Figure 9a shows the power provided by each CP to the vehicles as a function of the time referring to the St. C (figure on the left side) and SC (figure on the right side). The heat-map represents the power intensity that the EVs require from the CPs during the charge. The power variations depend on the modulation of both the onboard charger and the operations of the charging management system. The smoother power level variation that occurs near the end of the charging process of each EV is due to the decrease in the power resulting from the passage to the CV phase. Conversely, the more marked variation that occurs when another EV is connected or disconnected is due to the CMS operation that reduces or increases the consumption according to the St. C and SC operations. It is noteworthy that both CMSs start to modulate the power only if there are more than four EVs simultaneously under charging. This clearly appears in Figure 9a, in which the CMS operations become visible after the 5th EV is connected to CP_5.

From Figure 9a (left), it can be seen that the St. C evenly distributes the power to each vehicle. Since control of the t_{ech} is missing, the charging time depends on SOC_0 and N_{ch}; hence, the charging duration can present extremely varied values. In this case, the end-of-charging time occurs also when the operators are not available, causing the several visible downtimes between two consecutive charging events. The downtime periods are instead strongly reduced when the proposed SC is operated, as visible in Figure 9a (right).

By looking at Figure 9b it appears that, on average, the SC (right) provides the energy required to fully charge the EVs in less time with respect to the St. C (left). The average power P_{CH} obtained with the St. C method is about 73 kW. This value increases to 87.5 kW when the CH is managed by the SC method. As a result, the St. C takes about 16 h to charge all EVs, while the SC takes about 13.5 h. Since operators' work shifts end at 20:00, the SC allows them to fully charge more EVs during the daytime. This also allows operators to connect new EVs for overnight charging at the end of the working day. By observing the last set of eight vehicles in Figure 9a (left), it appears that no EVs complete the charging before 20:00. So, practically all of them go into overnight charging. On the other hand, as Figure 9a (right) shows, the SC makes it possible to charge five more EVs before 20:00,

allowing to connect five more EVs for overnight charging. Finally, considering the 24-h time window, the results show that the operators can perform 32 EV charges with the St. C method and can perform 37 charges with the SC method.

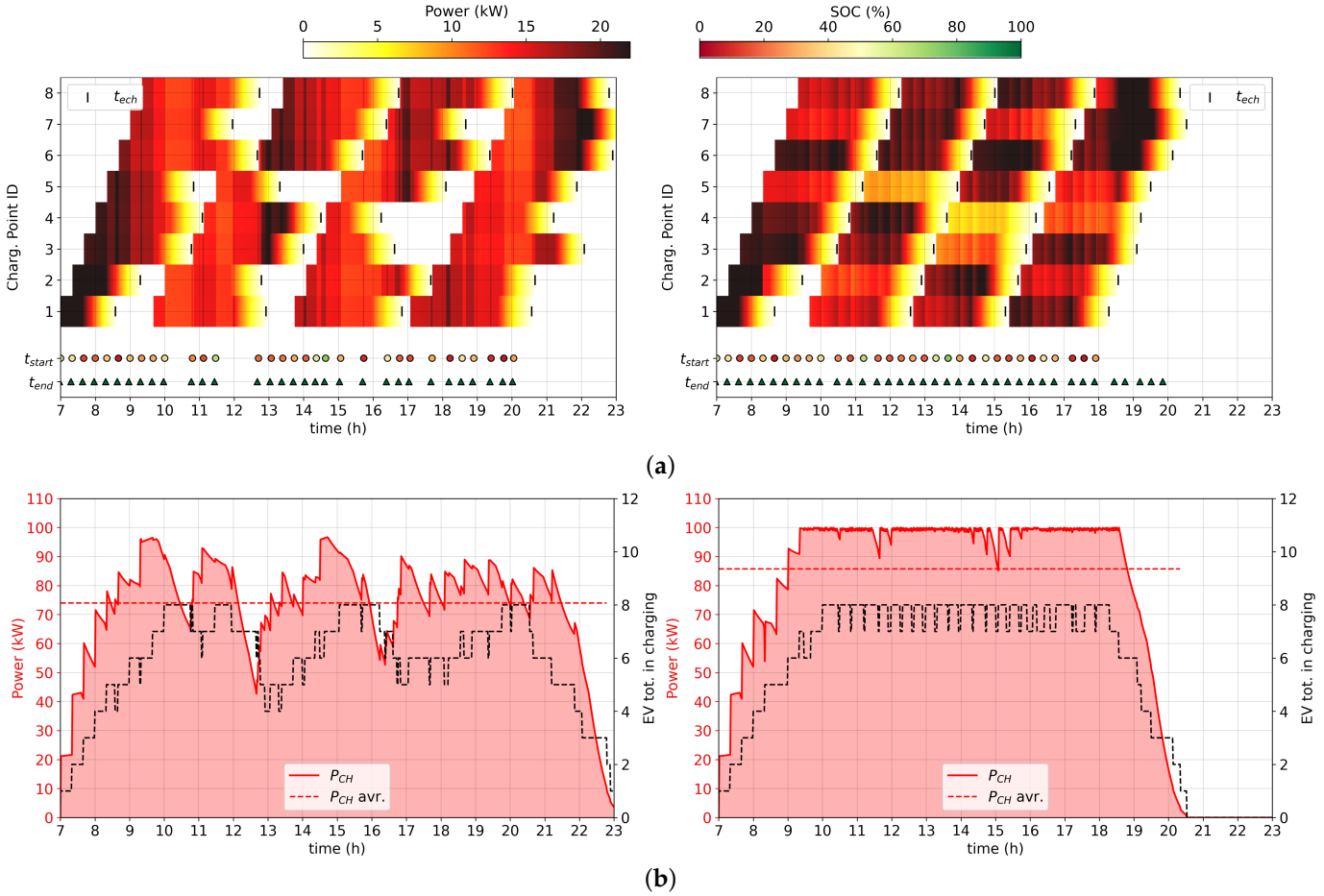

Figure 9. Power flow comparisons between the St.C (**left**) and the SC mode (**right**): (**a**) Heat-map of the power provided by each charging point (CP) during the charging events. The black bar markers indicate the end of charging, the round markers indicate the start of connection time, and the triangular markers indicate the end of connection time. The white band between the end of a charging process and a new connection to the same CP represents the downtimes. The markers on the bottom indicate the t_{start} and t_{end} of each charging process, whose color is a function of the vehicle's SOC. (**b**) Profile of the power required by the whole CH, the average value of which is indicated by the dashed red line. The black line represents the number of EVs simultaneously under charge.

The comparison is then extended to a broader time front of 10 days by measuring the following performance indicators:

1. Whole downtime of the CPs (T_{dw}).
2. CH power exploitation coefficient η_{exp} defined as $\bar{P}_{\text{CH}} / P_{\text{Chmax}}$, denoted as percentage.
3. The total number of charging events occurred within the 24-h period (i.e., the whole number of EVs connected per day).

The resulting values of the three performance indicators related to the 10 simulation days are reported in Figure 10.

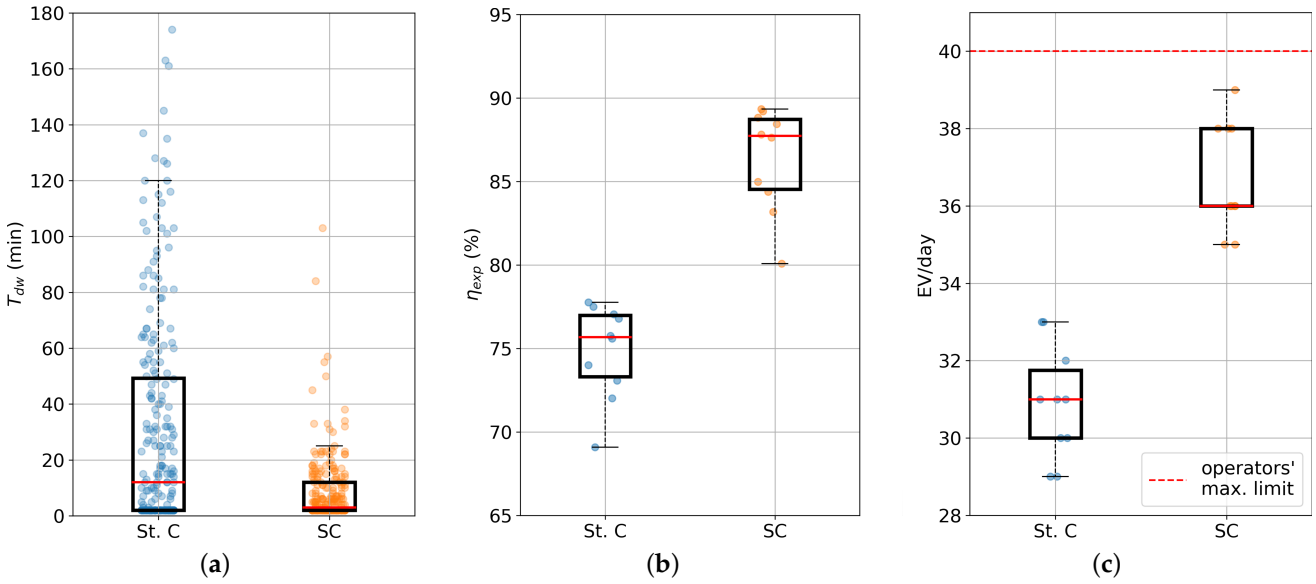

Figure 10. Comparison of the charging performances between St. C and SC considering 10 different days. (**a**) Downtime of each charging event at the CH. (**b**) Exploitation coefficient of the maximum power available at the CH. (**c**) Total number of charging events managed per day.

Figure 10a confirms the relevant reduction of the downtime obtained thanks to the proposed SC method. On average, EVs charged via SC remain plugged without adsorbing power for 8.7 min versus the 30.6 min of the St.C. 50% of EVs have a $T_{\mathrm{dw}} < 2$ min when the SC method is adopted versus the 12 min presented with St. C. Concerning the values of the power exploitation coefficient, Figure 10b shows the increase in the average power provided by the CH. The proposed SC allows better exploitation of the available maximum power showing a value of $\eta_{\mathrm{exp}} = 87\%$ versus the $\eta_{\mathrm{exp}} = 74\%$ obtained with the St.C. Finally, Figure 10c shows that the average number of charging events that occurred in the period of 24 h increased from 31 under St.C to 37 under SC. This number of charges becomes very close to the ideal maximum capability of 40 charges per day that two operators can perform.

In summary, the results confirmed the effectiveness of the proposed smart charging method for the ECS charging hub management that allowed us to obtain a decrease in T_{dw} of 71.5%, an increase in the power exploitation η_{exp} of 15.4%, and an increase in the number of charging events of 18.8%.

6. Conclusions

This paper addressed charging management for a car-sharing fleet based on battery electric vehicles. The analysis carried out on a real-world scenario (i.e., the electric car-sharing fleet of the city of Bologna) highlighted that the high variability of the charging duration (due to different arrival SOC) makes it challenging to plan the charging management entrusted to the operators. Often, an EV remains connected for longer than necessary as the end of charging occurs in periods when the ECS operator is not present (i.e., he is handling other vehicles). This leads to non-optimal exploitation of the charging hub as some charging points remain inactive even when a vehicle is connected. This also introduces a downtime. As a result, the average power used by the CH remains well below its maximum capability.

This paper addressed this issue by developing a smart charging method capable of minimizing the uncertainty of the duration of the charging and synchronizing it with the typical time schedule of the ECS operators. The proposed SC method acts on the management of the charging duration by controlling the power required by each single charging point according to the EV SOC and the desired end-of-charge time. At the same time, the proposed SC controls the total power consumption of the CH by preventing the power demand from exceeding the power available at the grid connection point. To

calculate the charging power set-point, a battery charging behavioral model was developed. The behavioral model was implemented starting from the measured charging profiles of the Renault ZOE. It forecasts the EV power demand as a function of the C-rate and SOC evolution during the charging process.

Finally, simulations were carried out considering a real case study scenario and comparing the performance of the SC with the standard charging method. The results showed that the proposed technique decreases the CPs downtime by 71.5% on average. This leads to better exploitation of the available contracted power with an increase of the average power from 74% to 87% of the maximum available level. The average number of vehicles that the same number of operators can fully charge during a working cycle increases by 18.8% (from 31 to 37 EVs per day) by using the proposed SC method.

It is worth remarking that these results are limited to the case study under consideration as described in Section 2. Different numbers of available CPs, a different level of power manageable by the CP as well as the maximum contracted power available to the whole CH, different EV models, more or fewer ECS operators, or a change in their work shifts may lead to different results. However, the models presented in the paper, as well as the proposed SC method, can be customized and adapted to different scenarios by opportunely setting the parameters of the equations presented in Sections 3.2 and 4.

Author Contributions: Conceptualization, F.L.F., M.R. and V.C.; methodology, F.L.F., M.R. and V.C.; software, F.L.F. and M.R.; validation, V.C., V.M. and M.R.; formal analysis, F.L.F., V.C., M.R. and V.M.; investigation, F.L.F.; writing—original draft preparation, F.L.F. and V.C.; writing—review and editing, F.L.F., V.C., M.R., V.M., J.L.A. and G.G.; visualization, F.L.F.; supervision, M.R., V.M., J.L.A. and G.G. All authors have read and agreed to the published version of the manuscript.

Funding: This research received no external funding.

Institutional Review Board Statement: This research received no external funding.

Informed Consent Statement: Not applicable.

Data Availability Statement: The original contributions presented in the study are included in the article; further inquiries can be directed to the corresponding author.

Acknowledgments: The authors would like to thank the company Tper-Trasporto Pubblico Emilia-Romagna and the Corrente Car Sharing for the assistance in developing this work. A heartfelt thanks also goes to Luca Astolfi for his time and support in providing and analyzing data.

Conflicts of Interest: The authors declare no conflict of interest.

Abbreviations

BCBM	Battery Charging Behavioral Model
CC-CV	Constant Current–Constant Voltage
CH	Charging Hub
CMS	Charging Management System
CP	Charging Point
ECS	Electric Car-Sharing
EV	Electric Vehicle
ID	Identification number
OD	Over-Day
ON	Over-Night
PWM	Pulse-Width Modulation
RES	Renewable Energy Sources
RMSE	Root-Mean-Square Error
SC	Smart Charging
St. C	Standard Charging
C_B	Battery energy capacity
C_R	Charging Rate
N_{ch}	Number of EV in charging

P_{CH}	Total power required by the CH
P_{EV}	Charging power of a single EV
SOC	State of Charge
SOC_0	Pre-charging SOC
SOC_{end}	Post-charging SOC

References

1. 2050 Long-Term Strategy. Available online: https://ec.europa.eu/clima/eu-action/climate-strategies-targets/2050-long-term-strategy{_}en (accessed on 9 September 2022).
2. Luo, C.; Ooi, B.T. Frequency deviation of thermal power plants due to wind farms. *IEEE Trans. Energy Convers.* **2006**, *21*, 708–716. [CrossRef]
3. Kroposki, B.; Johnson, B.; Zhang, Y.; Gevorgian, V.; Denholm, P.; Hodge, B.M.; Hannegan, B. Achieving a 100% renewable grid: Operating electric power systems with extremely high levels of variable renewable energy. *IEEE Power Energy Mag.* **2017**, *15*, 61–73. [CrossRef]
4. Lo Franco, F.; Ricco, M.; Mandrioli, R.; Grandi, G. Electric Vehicle Aggregate Power Flow Prediction and Smart Charging System for Distributed Renewable Energy Self-Consumption Optimization. *Energies* **2020**, *13*, 5003. [CrossRef]
5. Lo Franco, F.; Ricco, M.; Mandrioli, R.; Paternost, R.F.P.; Grandi, G. State of Charge Optimization-based Smart Charging of Aggregate Electric Vehicles from Distributed Renewable Energy Sources. In Proceedings of the 2021 IEEE 15th International Conference on Compatibility, Power Electronics and Power Engineering (CPE-POWERENG), Florence, Italy, 14–16 July 2021; IEEE: Piscataway, NJ, USA, 2021; pp. 1–6. [CrossRef]
6. Lo Franco, F.; Mandrioli, R.; Ricco, M.; Monteiro, V.; Monteiro, L.F.C.; Afonso, J.L.; Grandi, G. Electric Vehicles Charging Management System for Optimal Exploitation of Photovoltaic Energy Sources Considering Vehicle-to-Vehicle Mode. *Front. Energy Res.* **2021**, *9*, 642. [CrossRef]
7. Nour, M.; Said, S.M.; Ali, A.; Farkas, C. Smart Charging of Electric Vehicles According to Electricity Price. In Proceedings of the 2019 International Conference on Innovative Trends in Computer Engineering, ITCE 2019, Aswan, Egypt, 2–4 February 2019; pp. 432–437. [CrossRef]
8. Electric Vehicle Demand Response—ENTSO-E. Available online: https://www.entsoe.eu/Technopedia/techsheets/electric-vehicle-demand-response (accessed on 9 September 2022).
9. Integrated Smart GRID Cross-Functional Solutions for Optimized Synergetic Energy Distribution, Utilization Storage Technologies | InteGRIDy. Available online: http://www.integridy.eu/ (accessed on 9 September 2022).
10. Borge-Diez, D.; Icaza, D.; Açıkkalp, E.; Amaris, H. Combined vehicle to building (V2B) and vehicle to home (V2H) strategy to increase electric vehicle market share. *Energy* **2021**, *237*, 121608. [CrossRef]
11. Monteiro, V.; Monteiro, L.F.C.; Franco, F.L.; Mandrioli, R.; Ricco, M.; Grandi, G.; Afonso, J.L. The Role of Front-End AC/DC Converters in Hybrid AC/DC Smart Homes: Analysis and Experimental Validation. *Electronics* **2021**, *10*, 2601. [CrossRef]
12. Lazzeroni, P.; Cirimele, V.; Canova, A. Economic and environmental sustainability of Dynamic Wireless Power Transfer for electric vehicles supporting reduction of local air pollutant emissions. *Renew. Sustain. Energy Rev.* **2021**, *138*, 110537. [CrossRef]
13. Reche, C.; Tobias, A.; Viana, M. Vehicular Traffic in Urban Areas: Health Burden and Influence of Sustainable Urban Planning and Mobility. *Atmosphere* **2022**, *13*, 598. [CrossRef]
14. Karagulian, F.; Belis, C.A.; Dora, C.F.C.; Prüss-Ustün, A.M.; Bonjour, S.; Adair-Rohani, H.; Amann, M. Contributions to cities' ambient particulate matter (PM): A systematic review of local source contributions at global level. *Atmos. Environ.* **2015**, *120*, 475–483. [CrossRef]
15. Agarwal, P.; Sarkar, M.; Chakraborty, B.; Banerjee, T. Phytoremediation of Air Pollutants: Prospects and Challenges. In *Phytomanagement of Polluted Sites: Market Opportunities in Sustainable Phytoremediation*; Elsevier: Berlin/Heidelberg, Germany, 2018; pp. 221–241. [CrossRef]
16. Giesel, F.; Nobis, C. The Impact of Carsharing on Car Ownership in German Cities. *Transp. Res. Procedia* **2016**, *19*, 215–224. [CrossRef]
17. María Arbeláez Vélez, A.; Plepys, A.; Olsson, L.; Guyader, H. Car Sharing as a Strategy to Address GHG Emissions in the Transport System: Evaluation of Effects of Car Sharing in Amsterdam. *Sustainability* **2021**, *13*, 2418. [CrossRef]
18. Migliore, M.; D'Orso, G.; Caminiti, D. The environmental benefits of carsharing: The case study of Palermo. *Transp. Res. Procedia* **2020**, *48*, 2127–2139. [CrossRef]
19. Trend Europe: Electrification in car-sharing fleets-electrive.com. Available online: https://www.electrive.com/2020/03/08/trend-europe-electrification-in-car-sharing-fleets/ (accessed on 9 September 2022).
20. Electric Vehicle Car Sharing Platform | Interreg Europe—Sharing Solutions for Better Policy. Available online: https://www.interregeurope.eu/good-practices/electric-vehicle-car-sharing-platform (accessed on 9 September 2022).
21. Nicholas, M.; Bernard, M.R. Success Factors for Electric Carsharing. 2021. Available online: https://movmi.net/ (accessed on 9 September 2022).
22. He, L.; Ma, G.; Qi, W.; Wang, X. Charging an Electric Vehicle Sharing Fleet. *SSRN Electron. J.* **2019**, *23*, 471–487. [CrossRef]
23. Deza, A.; Huang, K.; Metel, M.R. Charging station optimization for balanced electric car sharing. *Discret. Appl. Math.* **2022**, *308*, 187–197. [CrossRef]

24. Wang, N.; Li, J.; Liu, X.; Guo, J. Study on the Charging Station Layout of Electric Car Sharing Mode. *Lect. Notes Electr. Eng.* **2022**, *769*, 785–802. [CrossRef]
25. Zhang, T.Z.; Chen, T.D. Smart charging management for shared autonomous electric vehicle fleets: A Puget Sound case study. *Transp. Res. Part D Transp. Environ.* **2020**, *78*. [CrossRef]
26. Ren, S.; Luo, F.; Lin, L.; Hsu, S.C.; LI, X.I. A novel dynamic pricing scheme for a large-scale electric vehicle sharing network considering vehicle relocation and vehicle-grid-integration. *Int. J. Prod. Econ.* **2019**, *218*, 339–351. [CrossRef]
27. Home Page of "Corrente" Web Site. Available online: https://corrente.app/#home (accessed on 5 September 2022).
28. Web Page of the Map of the Electric Car-Sharing Corrente in Bologna. Available online: https://corrente.app/pagina/estensionebologna/ (8 September 2022).
29. Schmenger, J.; Endres, S.; Zeltner, S.; März, M. A 22 kW on-board charger for automotive applications based on a modular design. In Proceedings of the 2014 IEEE Conference on Energy Conversion (CENCON), Johor Bahru, Malaysia, 13–14 October 2014; pp. 1–6. [CrossRef]
30. Shen, W.; Vo, T.T.; Kapoor, A. Charging algorithms of lithium-ion batteries: An overview. In Proceedings of the 2012 7th IEEE Conference on Industrial Electronics and Applications (ICIEA), Singapore, 18–20 July 2012; IEEE: Piscataway, NJ, USA, 2012; pp. 1567–1572. [CrossRef]
31. Lo Franco, F.; Ricco, M.; Mandrioli, R.; Viatkin, A.; Grandi, G. Current Pulse Generation Methods for Li-ion Battery Chargers. In Proceedings of the 2020 2nd IEEE International Conference on Industrial Electronics for Sustainable Energy Systems (IESES), Cagliari, Italy, 1–3 September 2020; IEEE: Piscataway, NJ, USA, 2020; Volume 1, pp. 339–344. [CrossRef]
32. Schaden, B.; Jatschka, T.; Limmer, S.; Raidl, G.R. Smart Charging of Electric Vehicles Considering SOC-Dependent Maximum Charging Powers. *Energies* **2021**, *14*, 7755. [CrossRef]
33. Vehicles-Fastned FAQ. Available online: https://support.fastned.nl/hc/en-gb/sections/4428932764573-Vehicles (accessed on 9 September 2022).
34. Renault-Fastned FAQ. Available online: https://support.fastned.nl/hc/en-gb/articles/360035723373-Renault (accessed on 9 September 2022).
35. Speak EV- Zoe Charge Curve-Mapped and Graphed. Available online: https://www.speakev.com/threads/zoe-q90-rapid-charge-curve-mapped-and-graphed.118785/ (accessed on 9 September 2022).
36. Speak EV- R90 v Q90 Charging Times. Available online: https://www.speakev.com/threads/r90-v-q90-charging-times.74249/ (accessed on 9 September 2022).
37. Speak EV-ZE50 versus ZE40-Renault Charging Data. Available online: https://www.speakev.com/threads/ze50-versus-ze40-renault-charging-data.152143/ (accessed on 9 September 2022).
38. IEC Technical Committee 69 IEC 61851-1:2017 Electric Vehicle Conductive Charging System-Part 1: General Requirements 2017. Available online: https://webstore.iec.ch/publication/33644 (accessed on 9 September 2022).